Upconversion in Er-implanted Al_2O_3 waveguides

G. N. van den Hoven, E. Snoeks,[a] and A. Polman
FOM–Institute for Atomic and Molecular Physics, Kruislaan 407, 1098 SJ Amsterdam, The Netherlands

C. van Dam, J. W. M. van Uffelen, and M. K. Smit
Delft University of Technology, Department of Electrical Engineering, Mekelweg 4, 2628 CD Delft, The Netherlands

(Received 2 August 1995; accepted for publication 1 November 1995)

When pumped with a 1.48 μm laser diode, Er-implanted Al_2O_3 ridge waveguides emit a broad spectrum consisting of several distinct peaks having wavelengths ranging from the midinfrared (1.53 μm) to the visible (520 nm). In order to explain these observations, three different upconversion mechanisms are considered: cooperative upconversion, excited state absorption, and pair-induced quenching. It is found that for samples with a high Er concentration (1.4 at. %), cooperative upconversion completely dominates the deexcitation of the Er^{3+} ions. For a much lower concentration (0.12 at. %), the influence of cooperative upconversion is strongly reduced, and another upconversion effect becomes apparent: excited state absorption. These conclusions are based on measurements of the luminescence emission versus pump intensity, and also on measured luminescence decay curves. The upconversion coefficient is found to be $(4\pm1)\times10^{-18}$ cm^3/s; the excited state absorption cross section is $(0.9\pm0.3)\times10^{-21}$ cm^2. It is shown that in spite of these upconversion effects, a high fraction of the Er^{3+} can be excited at low pump powers. For pump powers between 2 and 10 mW, the optimum Er concentration is calculated. The results show that for an Er concentration of 0.5 at. %, more than 2 dB/cm net optical gain is achievable at a pump power less than 10 mW. © *1996 American Institute of Physics.* [S0021-8979(96)08303-1]

I. INTRODUCTION

Erbium doping of planar optical waveguides has attracted much attention following the success of the erbium-doped fiber amplifier.[1–3] Trivalent erbium is used as optical dopant because of its intra-$4f$ transition around 1.54 μm, coinciding with the low-loss window of standard silica-based optical fiber. Optical waveguides doped with Er can therefore function as optical amplifiers in the standard telecommunications wavelength window around 1.55 μm, and be used to fabricate for instance lossless 3 dB splitters, and in general be used to compensate for the losses in a variety of passive and active components in an integrated optical device.

In the free Er^{3+} ion, the transitions around 1.53 μm are parity forbidden. Incorporating Er^{3+} in a solid host induces a weak mixing of states of opposite parity to the $4f$ electrons, which are shielded by filled $5s$ and $5p$ shells.[4] This results in allowed transitions, with radiative lifetimes for the excited states of up to several milliseconds, and emission and absorption cross sections of 10^{-20}–10^{-21} cm^2. The energy level diagram of Er^{3+} is schematically shown in Fig. 1. The lifetime of the first excited ($^4I_{13/2}$) state is long, and population inversion between this state and the ground state can in principle be achieved at relatively low pump powers. Because of the relatively small emission cross sections for Er^{3+}, reasonable values of optical gain (~3 dB=a factor of 2) can only be reached when the signal beam encounters a large amount of excited Er^{3+} (10^{20}–10^{21} cm^{-2}). For an integrated Er-doped amplifier in an optical circuit on a chip, the amplifier length is restricted to several centimeters for any useful application. This implies that Er concentrations in the range of 0.1–1 at. % are required.

At such high Er concentrations the distance between the Er^{3+} ions is small, and electric dipole–dipole interactions between the different ions take place, of which the interaction strength depends on $1/r^6$, with r the distance between two Er^{3+} ions. These interactions effectively lower the fraction of excited Er at a given pump power. The simplest form of such a concentration quenching effect is energy migration [see Fig. 1(a)], where an excited ion transfers its energy to a nearby ion in the ground state. This results in diffusion of the excitation, and finally loss of the excitation if one of the Er^{3+} ions couples to a defect, for example, a hydroxyl group.[5,6] Under conditions of amplification, most of the ions are excited to the first excited state, and another concentration quenching mechanism can take place: cooperative upconversion, also referred to as cross relaxation.[7–9] Figure 1(b) schematically shows this process, where two Er^{3+} ions, both in the first excited ($^4I_{13/2}$) state, interact, promoting one ion into the $^4I_{9/2}$ state, leaving the other in the ground state. Subsequently, the excited ion decays rapidly to the $^4I_{11/2}$ state through a nonradiative transition by emission of phonons.[10,11] From there it can decay either back to the first excited state or to the ground state. In effect, cooperative upconversion reduces the degree of inversion at a given pump power. Very efficient cooperative upconversion can occur when two (or more) ions form a pair (or cluster), resulting in almost immediate interaction of the ions once both of them are excited. This is referred to as pair-induced quenching (PIQ),[12–14] and effectively limits the maximum degree of inversion attainable in the material. Upconversion can also

[a]Present address: Philips Laboratories, 345 Scarborough Rd., Briarcliff Manor, NY 10510-2099.

 0021-8979/96/79(3)/1258/9/$6.00

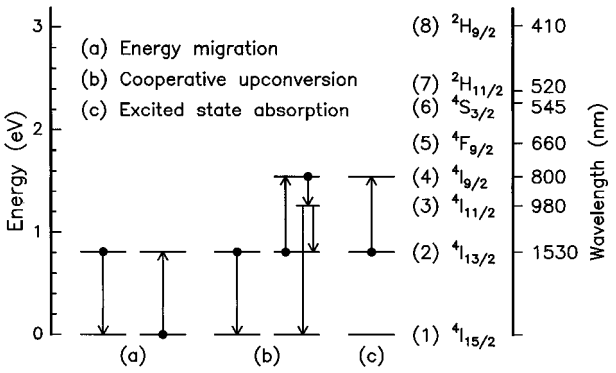

FIG. 1. Schematic of three different concentration quenching effects in Er^{3+}. The right-hand scale shows the Er^{3+} energy level diagram with the corresponding Russel–Saunders notation for the energy levels.

occur through absorption of a photon by an excited Er^{3+} ion, promoting it to a higher-energy state [see Fig. 1(c)]. This is generally referred to as excited state absorption (ESA).[15,16] This process is independent of Er concentration, as only one ion is involved, but depends on the pump intensity.

Although upconversion processes put a limit to the performance of optical amplifiers operating at 1.5 μm, they may be used to create higher-energy excitations, and thus shorter-wavelength photons, using relatively long-wavelength pump light. Several reports have shown this for bulk rare-earth-doped materials,[17–21] optical fibers,[22] as well as for planar waveguides.[23,24] This opens possibilities for the fabrication of visible and maybe even ultraviolet lasers pumped with readily available infrared pump sources.

In this work upconversion is studied in Er-doped Al_2O_3 planar waveguides which may be used for amplifiers and lasers operating at 1.53 μm. Polycrystalline γ-Al_2O_3 films were deposited on Si substrates by sputtering, and ridge waveguides made in these films show losses as low as 0.35 dB/cm. γ-Al_2O_3 has a cubic crystal structure very similar to that of Er_2O_3,[25] which may enable high concentration optical doping with Er. Such structural compatibility also might help to prevent clustering of Er, which has been shown to occur in SiO_2.[26] Photoluminescence studies of Er-implanted Al_2O_3 have shown Er^{3+} luminescence lifetimes as high as 6–10 ms, even for concentrations of $\sim$1 at. %.[27] This indicates that in this material the energy migration referred to in Fig. 1(a) does not result in luminescence quenching, presumably due to the absence of quenching centers.

In this study, it is found that Er-implanted Al_2O_3 ridge waveguides (Er concentrations of 0.12 and 1.4 at. %) pumped at 1.48 μm emit luminescence at several wavelengths shorter than the pump. Measurements of the luminescence intensity and decay rate, both versus pump intensity, show that both cooperative upconversion and ESA take place. The data are analyzed quantitatively, and the cooperative upconversion coefficient and ESA cross section are determined. Besides the first-order upconversion, also a second-order cooperative upconversion process is observed, which leads to green emission at 520 and 545 nm. From the determined coefficients and luminescence lifetimes, the optimum Er concentration for a planar Er-doped Al_2O_3 amplifier is deduced. It is concluded that net optical gain can be achieved in Er-implanted Al_2O_3 waveguides at pump powers below 10 mW.

II. EXPERIMENT

Al_2O_3 waveguide films, 600 nm thick, were fabricated by radio-frequency magnetron sputter deposition from an Al_2O_3 target onto a thermally oxidized Si (100) substrate. The deposition was carried out in an oxidizing ambient of 90% Ar and 10% O_2 at a pressure of 0.8 Pa, with the substrate held at room temperature. This process is known to produce dense stochiometric cubic polycrystalline Al_2O_3 films.[28,29] Subsequently, two samples were implanted with Er, with the samples held at 77 K. One sample, referred to as the high-concentration sample, was implanted with 1.3 MeV Er to a fluence of 1.62×10^{16} Er/cm^2. The other, referred to as the low-concentration sample, was implanted at four different energies between 180 keV and 1.3 MeV to a total fluence of 5.1×10^{15} Er/cm^2.

Using Rutherford backscattering spectrometry (RBS), the Er fluence was confirmed and the Er depth profiles were measured. The high-concentration sample shows a Gaussian Er profile peaked at a depth of 270 nm with a full width at half-maximum of 160 nm. The Er peak concentration is 1.4 at. %. The low-concentration sample shows a roughly constant Er concentration of 0.12 at. % ranging from just under the Al_2O_3 surface to a depth of $\approx$400 nm.

After implantation, waveguides were defined by photolithographic patterning of the sample with stripes having widths ranging from 1.0 to 3.5 μm. An Ar atom beam was used to etch 300 nm of the Al_2O_3, resulting in ridge waveguides under the previously defined stripes. Following this, a top SiO_2 cladding layer was deposited, and the structure was annealed at either 825 or 775 °C for 1 h. This annealing treatment results in low loss waveguides (0.35 dB/cm),[29] and is also necessary to anneal out implantation damage and activate the Er.[27] Finally, the samples were saw cut to $\approx$9 mm length, and the end faces were mechanically polished in order to attain optimal light coupling into the waveguide.

Photoluminescence (PL) spectroscopy was performed by coupling a 1.48 μm InGaAsP laser diode pump into the waveguides using a tapered optical fiber, which was aligned to the waveguides using piezoelectric actuators. Thus, powers of up to 5 mW could be coupled into the guides, resulting in pump intensities of up to 2×10^5 W/cm^2. The luminescence emitted by the waveguides was collected using a fiber with a 0.8-mm-diam core mounted normal to the sample surface. The luminescence was then dispersed using a 48 cm single-grating monochromator and detected with either a liquid-nitrogen-cooled Ge detector, for the infrared, or a cooled photomultiplier tube (PMT), for the visible and near-infrared part of the spectrum. The pump laser was mechanically chopped, and lock-in techniques were employed to monitor the signal. All luminescence intensities were corrected for detector sensitivities, and their relative strengths may be compared in terms of photons/nm. The time evolution of the luminescence was measured using an averaging

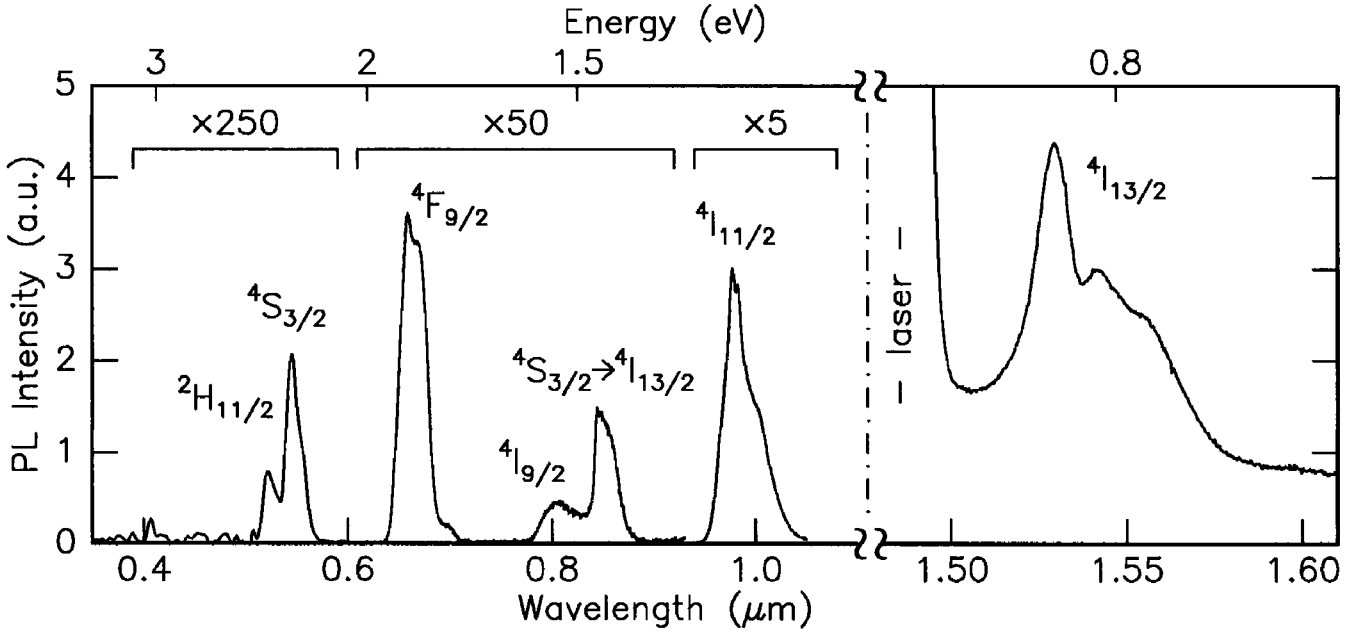

FIG. 2. Photoluminescence spectrum of an Er-implanted Al_2O_3 ridge waveguide pumped with a 1.48 μm laser diode. The transitions are indicated by their initial states. All but one of the transitions terminate at the ground state; the one exception is also indicated by its final state. Note the multiplication factors ($\times 5$, $\times 50$, $\times 250$). The relative intensities may be compared.

digitizing oscilloscope. All measurements were performed at room temperature.

III. RESULTS AND DISCUSSION

A. Photoluminescence

Figure 2 shows the PL spectrum obtained by coupling 2 mW of 1.48 μm pump light into a 1.5-μm-wide Er-implanted Al_2O_3 waveguide (high-concentration sample: 1.4 at. %). The luminescence peak around 1.53 μm is characteristic for emission of Er^{3+} in its first excited state,[4] and has been seen before in Er-implanted Al_2O_3.[27] The peak at 1.48 μm is due to scattering of pump laser light. In addition, several other luminescence peaks can be distinguished, each one characteristic of an intra-4f transition in Er^{3+}, as indicated in the figure. The occurrence of these emission peaks is indicative of upconversion. In particular, viewing the sample through an optical microscope shows bright green emission by the waveguide.[30,31]

The different upconversion mechanisms introduced in Sec. I each depend in a characteristic way on the pump power in the waveguide. In order to determine which of these mechanisms is responsible for the observed upconversion luminescence, the luminescence intensity of the different peaks was measured as a function of pump power. Note that the luminescence intensity of a peak in the PL spectrum is directly related to the concentration of Er^{3+} ions in the excited state corresponding to that emission. In the following such measurements are shown for two cases: high and low Er concentration.

B. High Er concentration

Figure 3 shows the intensity of the 980 nm luminescence, as observed in Fig. 2, versus the 1.53 μm intensity, on logarithmic scales. Data were obtained by varying the pump power between 0.03 and 5 mW. The data show a linear behavior with a slope of 1.89(1). Also shown in the figure is the calculated behavior of the 980 nm emission for three cases, as follows.

(1) Cooperative upconversion [see also Fig. 1(b)]: Two ions in the first excited state ($^4I_{13/2}$) interact to populate the $^4I_{9/2}$ state, and from there the $^4I_{11/2}$ state is populated due to rapid nonradiative decay. The rate of cooperative upconversion depends quadratically on the concentration of ions in the $^4I_{13/2}$ state. Therefore, the 980 nm intensity versus that at 1.53 μm should give a slope of two in Fig. 3 (solid line).

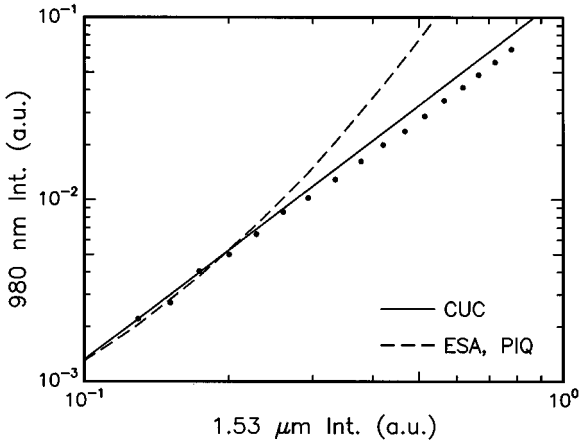

FIG. 3. Luminescence intensity at 980 nm vs that at 1.53 μm for the high-concentration sample (1.4 at. % Er), on logarithmic scales (solid dots). The calculated behavior of three possible upconversion mechanisms is shown: cooperative upconversion (CUC), excited state absorption (ESA), and pair-induced quenching (PIQ).

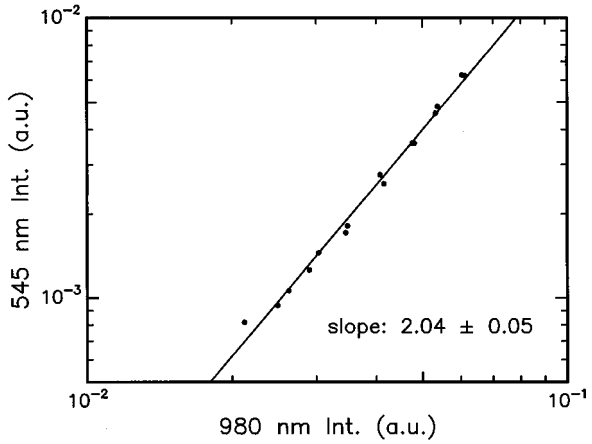

FIG. 4. Luminescence intensity at 545 nm vs that at 980 nm for the high-concentration sample (1.4 at. % Er), on logarithmic scales (solid dots). A linear fit through the data is shown.

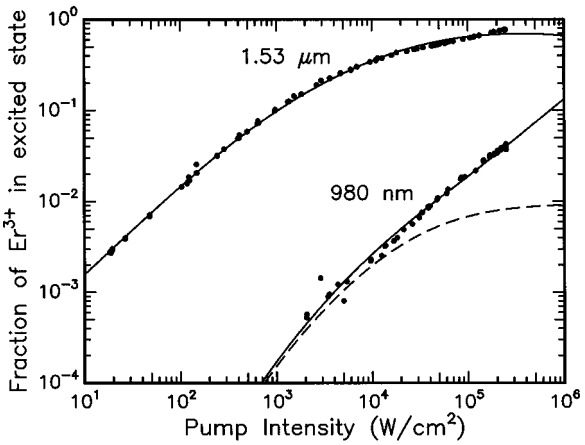

FIG. 5. Population fractions of Er^{3+} in the $^4I_{13/2}$ state (1.53 μm) and $^4I_{11/2}$ state (980 nm) vs pump intensity for the low-concentration sample (0.12 at. % Er) on logarithmic scales (solid dots). The solid lines are fits to the data including effects of cooperative upconversion and excited state absorption. The dashed line shows the effect on the 980 nm luminescence of cooperative upconversion only.

(2) Excited state absorption [see also Fig. 1(c)]: One Er^{3+} ion in the $^4I_{13/2}$ state absorbs a 1.48 μm pump photon, thus populating the $^4I_{9/2}$ state. This process depends on the concentration of ions in the $^4I_{13/2}$ state and the pump intensity. Therefore, the 980 nm emission will be proportional to the product of the 1.53 μm emission times and the pump intensity. The dashed line in Fig. 3 shows this behavior, where the vertical scaling was adjusted in order to overlay the low pump power data.

(3) Pair-induced quenching: The same scheme applies as for cooperative upconversion [Fig. 1(b)]. Because the interaction occurs instantaneously as soon as both ions in a pair are excited, the rate of this process depends on the concentration of excited pairs in which one ion is already excited, and the pump intensity, which excites the second ion. This results in the same dependence as expected for ESA.

Clearly, the data in Fig. 3 are quite close to the expected behavior for cooperative upconversion, and deviate strongly from what is expected for ESA and pair-induced quenching. It is therefore concluded that for this high-concentration sample cooperative upconversion is the main mechanism leading to the luminescence at 800 and 980 nm.

Figure 4 shows the 545 nm emission also seen in Fig. 2 versus that at 980 nm on logarithmic scales. Data were obtained by varying the pump power between 0.5 and 5 mW. Again, a straight line is found and a linear fit yields a slope of 2.04(5). Here it is concluded that cooperative upconversion of two ions in the $^4I_{11/2}$ state populates the $^2H_{11/2}$ state. This explains the visible luminescence peaks in Fig. 2: The green emission peak at 520 nm arises from luminescence due to a transition from the $^2H_{11/2}$ state to the ground state, while the emission at 545 and 660 nm is caused by nonradiative decay from the $^2H_{11/2}$ state to the $^4S_{3/2}$ and the $^4F_{9/2}$ states, followed by radiative decay to the ground state. In addition, a luminescence peak at 850 nm is observed, due to radiative decay from the $^4S_{3/2}$ to the $^4I_{13/2}$ state.

The occurrence of this second-order upconversion process also explains why the slope of the 980 nm intensity versus the 1.53 μm intensity (Fig. 3) is slightly less than 2: The second-order cooperative upconversion depletes the population of the level which emits the 980 nm light, resulting in a slope smaller than 2 for the data in Fig. 3.

C. Low Er concentration

The upconversion behavior of the high Er concentration sample is completely dominated by cooperative upconversion. In order to reduce this, and in order to study other possible upconversion mechanisms, a sample was fabricated with a much lower (0.12 at. %) Er concentration. This sample exhibits a luminescence spectrum similar to that in Fig. 2, but now the intensities of the higher-order emission peaks are strongly reduced. In particular, the bright green luminescence emitted by the high-concentration sample is now barely visible to the eye.

Figure 5 shows the 1.53 μm and 980 nm luminescence intensities observed in the low-concentration sample as a function of pump intensity, on logarithmic scales. The luminescence intensity at each wavelength is proportional to the fraction of excited Er^{3+} ions in the corresponding energy level, and the measured data have been converted to these fractions as is discussed hereafter. The luminescence around 1.53 μm, originating from the first excited state, initially shows a linear dependence on pump intensity, i.e., a slope of 1 in Fig. 5. As higher intensities are reached, the luminescence deviates from the linear behavior and eventually saturates. This is expected because the population of Er^{3+} ions in the ground state is depleted, and less Er^{3+} is left to be excited. Above the pump intensity where the 1.53 μm emission starts to deviate from a straight line, luminescence around 980 nm ($^4I_{11/2}$) appears. Its intensity increases much more strongly with pump power than the 1.53 μm emission in this range.

The behavior shown in Fig. 5 can be modeled by solving rate equations which govern the populations in each level,

$$\frac{dN_1}{dt} = -N_1R_{12} + N_2R_{21} + \frac{N_2}{\tau_2} + C_{24}N_2^2, \tag{1}$$

$$\frac{dN_2}{dt} = +N_1R_{12} - N_2R_{21} - \frac{N_2}{\tau_2} + \frac{N_3}{\tau_3} - 2C_{24}N_2^2 - N_2R_{24}, \tag{2}$$

$$\frac{dN_3}{dt} = -\frac{N_3}{\tau_3} + \frac{N_4}{\tau_4}, \tag{3}$$

$$\frac{dN_4}{dt} = -\frac{N_4}{\tau_4} + C_{24}N_2^2 + N_2R_{24}, \tag{4}$$

where N_{1-4} are the Er^{3+} concentrations in the first four energy levels (see Fig. 1). The total Er concentration is denoted N_0. Furthermore, R_{12} is the pump rate, R_{21} is the rate of stimulated emission of the pump, τ_2 and τ_3 are the luminescence lifetimes of levels 2 and 3, and t is time. It is assumed that all population in level 3 decays nonradiatively to level 2. This is a realistic assumption which is confirmed later on. Cooperative upconversion has been included by introducing the quadratic terms with coefficient C_{24} for upconversion from level 2 to 4; excited state absorption is included through the rate R_{24}. The rates R_{ij} are equal to $I\sigma_{ij}/h\nu$, with I the pump intensity, σ_{ij} the cross section, and $h\nu$ the pump photon energy. Here, σ_{12} is the pump absorption cross section, σ_{21} is the cross section for stimulated emission at the pump wavelength, and σ_{24} is the cross section for ESA. When solving the rate equations the population of level 4 can be neglected as it rapidly decays to level 3 nonradiatively. Also neglected is the population of the higher-lying levels, e.g., the weak green luminescence, as it is small for this low-concentration sample. Note that amplified spontaneous emission may also be neglected for this short sample length (<9 mm).

Under steady-state conditions all time derivatives are zero, and solving Eqs. (2)–(4) leads to an expression for the dependence of N_2 (1.53 μm emission) on pump intensity,

$$N_2 = \frac{-b + \sqrt{b^2 - 4ac}}{2a}, \tag{5}$$

with

$$a = C_{24}(1 + \tau_3 R_{12}),$$

$$b = 1/\tau_2 + R_{12} + R_{21} + \tau_3 R_{12} R_{24},$$

$$c = -N_0 R_{12}.$$

The lifetime τ_2 was measured to be 7.8 ms, and σ_{12} and σ_{21} at the pump wavelength of 1.475 μm are 2.7×10^{-21} and 0.77×10^{-21} cm^2, respectively.[32] The lifetime τ_3 was determined to be 30 μs (see Sec. III D). Equation (5) was fitted through the measured 1.53 μm luminescence data in Fig. 5 (solid line), with C_{24}, the collection efficiency, and the absolute pump intensity as a free parameters. The best fit is obtained for $C_{24} = (4\pm1)\times10^{-18}$ cm^3/s. As Eq. (5) gives the absolute population of Er^{3+} ions in the first excited state, the fit through the data can be used to convert the measured PL intensity to a population scale. This has been done in Fig. 5, where the left-hand scale shows the fraction of Er^{3+} ions in the excited state. As can be seen, for the highest pump intensity used in the measurement, the population in the first excited state is 70%. Note that the maximum achievable degree of inversion at this pump wavelength is limited to 78% due to stimulated emission of the pump.

Solving Eqs. (3) and (4) in steady state gives an expression for N_3 (980 nm) vs N_2 (1.53 μm),

$$N_3 = \tau_3(C_{24}N_2^2 + N_2R_{24}). \tag{6}$$

Using the dependence of N_2 on pump intensity as determined above, N_3 can now also be determined, the unknown parameter in Eq. (6) being R_{24}, which contains the cross section for ESA. This parameter determines the slope of the curve for the 980 nm data in Fig. 5 at high pump intensities. From the fit of this curve, it is found that $\sigma_{24} = (0.9\pm0.3)\times10^{-21}$ cm^2. The absolute normalization of the data is determined by the radiative decay rate of the transition and the collection efficiency. Because the collection efficiency is known from the fit to the 1.53 μm data, fitting the 980 nm data yields the radiative decay rate of the 980 nm luminescence: 300 s^{-1}. This rate is much lower than the total decay rate of the 980 nm luminescence (3.3×10^4 s^{-1}), confirming our assumption that nonradiative decay to the first excited state dominates the decay of the $^4I_{11/2}$ state. Just as for the 1.53 μm data, the 980 nm PL intensities were converted to populations, so that the left-hand axis in Fig. 5 also gives the fraction of Er^{3+} ions in level 3. Note that if the 980 nm emission would be a result of cooperative upconversion only ($R_{24}=0$), N_3 should depend quadratically on N_2 [see Eq. (6)]. Such behavior is indicated in the figure by the dashed line, and clearly does not fit the data. Therefore, for this low-concentration sample, both ESA as well as cooperative upconversion determine the total upconversion behavior.

Further note that although pair-inducing quenching could give rise to similar effects as just ascribed to ESA, it is ruled out on the basis of the measurements shown in Fig. 3: Because the high Er concentration sample shows no evidence for pair-induced quenching, it is unlikely that this effect would occur in the sample with a ten times lower Er concentration.

D. Time evolution

An independent method of determining the upconversion mechanism is by measuring the luminescence decay upon switching off the pump light.[33–35] Figure 6 shows the 1.53 μm luminescence decay after pumping to steady state for several different pump intensities in the low-concentration sample. At low intensities the decay is a single exponential; the lifetime of the population of the $^4I_{13/2}$ state is 7.8 ms. At higher intensities the data show an initial nonexponential decay. Such behavior may be explained in terms of cooperative upconversion, which continues to deplete the first excited state even after the pump is switched off. In this case, the depletion rate depends on the population, resulting in nonexponential decay. As both ESA and pair-induced quenching depend on the presence of a pump beam, these mechanisms do not affect the decay rate.

The decay curves may be described by solving Eq. (2), with the pump rates set to zero, and neglecting the influence of level 3 (which is justified considering that $\tau_2 \gg \tau_3$),

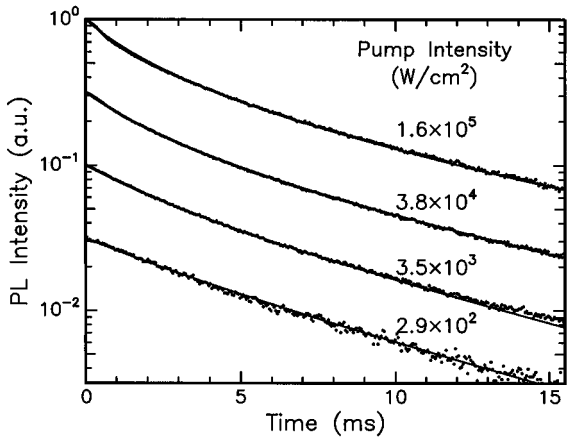

FIG. 6. Luminescence decay curves measured at 1.53 μm (dots) after pumping to steady state and switching off the pump source for four different 1.48 μm pump intensities. The curves are offset with respect to each other for clarity. The data are for the low-concentration sample (0.12 at. % Er). Fits to the data are shown as solid lines.

$$N_2(t)=\frac{N_2(0)}{[1+N_2(0)C_{24}\tau_2]\exp(t/\tau_2)-N_2(0)C_{24}\tau_2}, \tag{7}$$

where $N_2(0)$ is the Er^{3+} population in level 2 at the moment the pump was switched off. The photoluminescence decay traces in Fig. 6 were fitted using Eq. (7), yielding values for τ_2 and $N_2(0)C_{24}$. From the latter, the upconversion coefficient was extracted by evaluating $N_2(0)$ from Fig. 5 for each pump intensity in Fig. 6. This analysis was performed for four decay traces taken at different pump intensities, and consistently resulted in $C_{24}=(4\pm1)\times10^{-18}$ cm^3/s. This result is in perfect agreement with the value for the upconversion coefficient found in the previous subsection.

Figure 7 shows the luminescence decay of the 980 nm emission after pumping at an intensity of 5×10^4 W/cm^2. Here the time scale is much shorter than in Fig. 6 (μs instead of ms). Initially the decay proceeds very rapidly, then the decay rate decreases, and after 300 μs still 30% of the original population is present. This is due to the two different

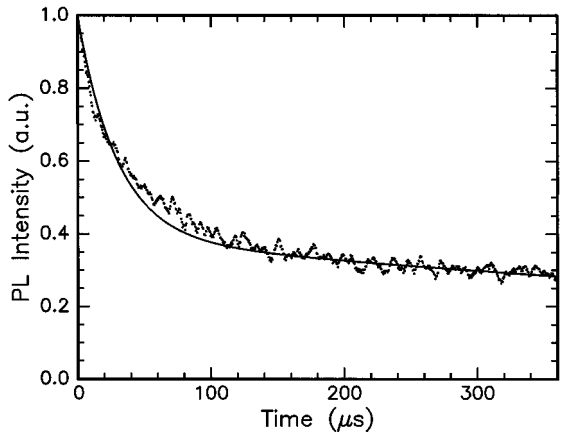

FIG. 7. Luminescence decay of the 980 nm luminescence (dots) after switching off the pump source for a pump intensity of 5×10^4 W/cm^2. The data are for the low-concentration sample (0.12 at. % Er). The solid line is a fit to the data.

mechanisms which populate the $^4I_{11/2}$ state: ESA and cooperative upconversion. At the moment that the pump is switched off ESA stops, and the Er population that was excited through ESA will decay with the lifetime of the $^4I_{11/2}$ state. Cooperative upconversion, however, continues to populate this state even after the pump has been switched off due to the long lifetime of the first excited state. Therefore, a long tail can be observed in the 980 nm decay. The ratio between the intensities of the fast and slow decay components of the 980 nm light reflects the contributions of each upconversion mechanism to the population of the $^4I_{11/2}$ state: $\approx$60% by ESA and $\approx$40% by cooperative upconversion. Quantative analysis of the decay curve is obtained by solving Eqs. (2) and (3) numerically. The result is shown in Fig. 7 as the solid line. From this fit, the lifetime of the third excited state is deduced: $\tau_3=30$ μs. Comparing this number to typical radiative decay rates for Er^{3+} (several ms) indicates that the decay of the $^4I_{11/2}$ energy level is dominated by multiphonon emission rather than radiative decay.

E. Understanding the coefficients

The coefficients for cooperative upconversion and excited state absorption depend strongly on the exact locations of the Er^{3+} energy levels. For instance, in the case of cooperative upconversion, the combined energies of two excited Er^{3+} ions must equal the energy of the higher-lying acceptor level in order to obtain resonant excitation of this level. For ESA, the energy of an excited Er^{3+} ion added to the pump photon energy must equal this higher-lying energy level.

The relative probabilities of these processes may be calculated by performing the convolution of two energy distributions. The energy distribution of Er^{3+} in the first excited state can be represented by the emission cross section as a function of wave number, $\sigma_{21}(k)$. Thus, the probability of exciting an energy level at wave number k through cooperative upconversion $\varphi_{\mathrm{CUC}}(k)$ is related to the convolution of two first excited state emission spectra,

$$\varphi_{\mathrm{CUC}}(k)=\int \sigma_{21}(k')\sigma_{21}(k-k')dk'. \tag{8}$$

For ESA the probability of excitation to some energy level at wave number k is related to

$$\varphi_{\mathrm{ESA}}(k)=\int \sigma_{21}(k')\sigma_{\mathrm{laser}}(k-k')dk', \tag{9}$$

with σ_{laser} the emission spectrum of the pump laser.

Figure 8 shows both $\varphi_{\mathrm{CUC}}(k)$ and $\varphi_{\mathrm{ESA}}(k)$, calculated using Eqs. (8) and (9) from the known Er emission and laser spectra. Also shown is the emission spectrum of the $^4I_{9/2}\rightarrow{}^4I_{15/2}$ (acceptor state to ground state) transition. Clearly, the maximum of $\varphi_{\mathrm{CUC}}(k)$ does not coincide with the energy of the $^4I_{9/2}$ level, indicating that cooperative upconversion from the first excited state is not quite resonant with the $^4I_{9/2}$ energy level. Nevertheless, in the experiments described above, cooperative upconversion is observed, leading to the indication that excitation of this level is a phonon-assisted process, i.e., the surplus of energy for excitation of the $^4I_{9/2}$ energy level is dissipated by the emission of a pho-

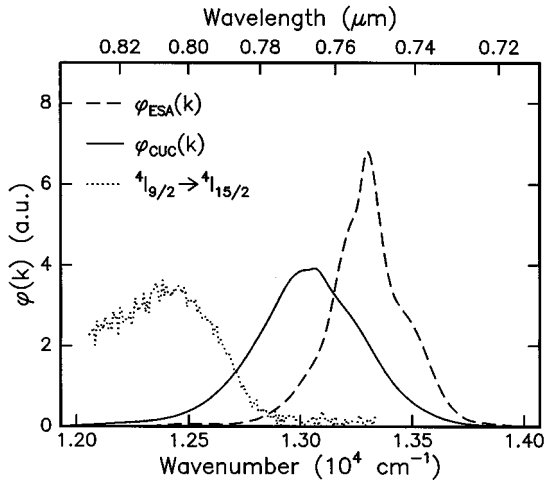

FIG. 8. The convolution of two identical Er^{3+} emission spectra, $\varphi_{CUC}(k)$, and of the Er^{3+} emission spectrum with the pump spectrum, $\varphi_{ESA}(k)$, vs wave number k. These curves give a measure for the probability of cooperative upconversion (CUC) and excited state absorption (ESA). Also shown is the measured emission spectrum of the $^4I_{9/2}\rightarrow{}^4I_{15/2}$ transition.

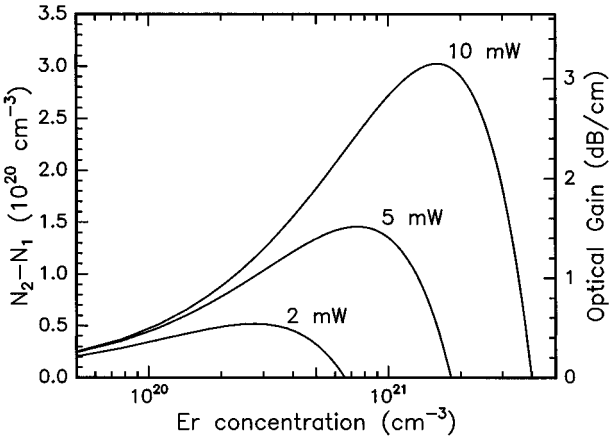

FIG. 9. Difference between the concentration Er in the first excited state and that in the ground state, N_2-N_1, vs the concentration of Er in an Al_2O_3 waveguide. The right-hand axis shows the corresponding net optical gain at 1.53 μm for an Al_2O_3 waveguide with 40% of the signal confined to the core of the guide. The calculations are performed for three different pump powers indicated in the figure, and may be used to determine the optimum Er concentration for a given pump power.

non. $\varphi_{ESA}(k)$ is even less resonant with the $^4I_{9/2}$ energy level. Therefore, if ESA is to occur, the energy gap of $\sim$1000 cm^{-1} between $\varphi_{ESA}(k)$ and the $^4I_{9/2}$ energy level must also be bridged by phonon emission.

In Al_2O_3 such phonon-assisted processes are possible because the highest phonon energy is 870 cm^{-1} (0.1 eV) for transverse optical phonons.[36] Therefore, roughly one phonon is necessary for these processes, so that probability for upconversion and ESA may still be appreciable, but considerably lower than for resonant excitation. Indeed, the ESA cross section determined in Sec. III C is nearly a factor of 10 smaller than the maximum absorption cross section for excitation of the first excited state. The ESA cross section of 0.9×10^{-21} cm^2 found here is comparable to that measured in erbium-doped fiber amplifiers (0.5×10^{-21} cm^2).[37]

The main conclusion from Fig. 8 is that the phonon spectrum of the host material plays an important role in determining the strength of cooperative upconversion and excited state absorption. Lowering the phonon energy by addition of heavy elements might help to lower the upconversion coefficients, thereby reducing their effect on the performance of amplifiers and lasers. On the other hand, a lower phonon energy would also result in a longer lifetime for the $^4I_{11/2}$ energy level, causing a buildup of population in this level, reducing the optical amplification around 1.53 μm. There are only a few measurements of cooperative upconversion coefficients (C_{24}) in other materials. Comparing the coefficient of 4×10^{-18} cm^3/s measured here for Er in Al_2O_3 to those materials, shows that C_{24} for Er in Al_2O_3 is one of the lowest. For instance, for Er-doped yttrium aluminum garnet (YAG), which has a similar crystal structure as Al_2O_3, $C_{24}=5.4\times10^{-17}$ cm^3/s,[18] much higher than for Al_2O_3. For soda-lime glass, $C_{24}=3\times10^{-18}$ cm^3/s, nearly the same as for Al_2O_3.[35] Recent measurements on two other silica-based glasses show $C_{24}=1-10\times10^{-18}$ cm^3/s.[38] In contrast, Er-doped fused silica codoped with Ge, Al, and P, a glass typically used for fiber amplifiers, shows a much higher C_{24} of 10^{-16} cm^3/s.[8] Also, Er-implanted phosphorous silicate glass (P glass), a material considered to be a candidate for optical amplifiers, shows a high C_{24} of 9×10^{-17} cm^3/s.[39]

F. Optimum Er concentration for an optical amplifier operating at 1.53 μm

In the previous subsections it became clear how cooperative upconversion and ESA influence the population of the different energy levels of Er^{3+}. The coefficients determined in Sec. III C may now be used to calculate the optimum Er concentration for an Er-doped optical amplifier operating at 1.53 μm. The optical gain is given by $\sigma_{21}N_2-\sigma_{12}N_1$ times the fraction of signal light which propagates in the core of the waveguide. At 1.53 μm $\sigma_{21}\approx\sigma_{12}$, so that the important parameter becomes N_2-N_1. Note that N_2 and N_1 are concentrations, not relative populations.

Figure 9 shows calculations of N_2-N_1 versus the Er concentration in an Al_2O_3 waveguide for three different pump powers, based on all the parameters and rate equations introduced above. The right-hand axis shows the corresponding net optical gain at 1.53 μm (excluding waveguide loss). The Er concentration is assumed to be constant within the core of the guide, and 40% of the signal is confined in the core. It is apparent that for each pump power there is an optimum Er concentration, which increases with increasing pump power. For small values of the pump powers the maximum achievable optical gain is small. Also, above a certain concentration threshold the optical gain begins to decrease because there is not enough pump power to excite all the Er^{3+}. The higher the pump power, the higher this concentration threshold, and the higher the optical gain. Figure 9 shows that high values of optical gain at 1.53 μm (0.5–3 dB/cm) can be achieved even for low pump powers (2–10 mW). This is because of the relatively high cross sections for Er^{3+} in Al_2O_3,[32] and lifetime,[27] combined with the high in-

tensities of pump and signal beams in the waveguide. Note that the calculations are performed in the small signal limit, i.e., the signal power is much smaller than the pump.

For a realistic pump power of less than 10 mW and an Er concentration of 5×10^{20} Er/cm^3 (0.5 at. %), more than 2 dB/cm net optical gain is achievable. This would be the highest net optical gain for the lowest pump power reported for Er-doped planar waveguides.[40–44] Note that for realistic amplifiers, the pump power decreases as it propagates through the waveguide. Therefore, the ideal Er concentration for a given pump power will be somewhat lower than shown in Fig. 9. Similar calculations as performed above have also been done for Er-doped glass waveguide amplifiers, showing that in these materials similar gain results are only achievable for pump powers in excess of 100 mW,[45] too much for many applications. Recent experiments in our laboratory on 4-cm-long Al_2O_3 waveguides with 0.3 at. % Er have shown a net optical gain of 2 dB (including 0.4 dB/cm waveguide loss) for an input pump power of 10 mW; this value of optical gain agrees well with a full calculation of the evolution of pump and signal using the models described in this study.[46,47]

IV. CONCLUSIONS

In conclusion, Er-implanted Al_2O_3 planar waveguides pumped with 1.48 μm light from a semiconductor diode laser show a broad luminescence spectrum with multiple peaks ranging from 520 nm to 1.53 μm due to upconversion. For high Er concentrations ($\sim$1 at. %) cooperative upconversion due to Er–Er interactions is found to dominate; for lower Er concentrations ($\sim$0.1 at. %) this effect is much less strong, and excited state absorption becomes apparent. From measurements of the luminescence intensities versus pump intensity, the coefficient for cooperative upconversion is found to be $(4\pm1)\times10^{-18}$ cm^3/s. The $^4I_{13/2}\rightarrow{}^4I_{9/2}$ excited state absorption cross section is $(0.9\pm0.3)\times10^{-21}$ cm^2. Both upconversion processes are due to phonon-assisted excitation of the third excited state of Er^{3+} ($^4I_{9/2}$). From all the parameters determined, the optimum Er concentration was determined for an Er-implanted Al_2O_3 planar waveguide amplifier operating at 1.5 μm. For a low pump power of 10 mW in the waveguide and an Er concentration of $\sim5\times10^{20}$ cm^{-3} (0.5 at. %) more than 2 dB/cm net optical gain is achievable.

ACKNOWLEDGMENTS

The authors would like to thank E. Radius for help in building the waveguide coupling setup and R. J. I. M. Koper for mechanical polishing of the waveguides. A. M. Vredenberg is thanked for useful discussions concerning upconversion mechanisms. B. H. Verbeek from the Philips Optoelectronic Center is acknowledged for supplying the high-power InGaAsP 1.48 μm pump laser. Work at the FOM–Institute was part of the research program of the Foundation for Fundamental Research on Matter (FOM), and was made possible by financial support from the Dutch Organization for the Advancement of Research (NWO), the IC Technology Program (IOP Electro-Optics) of the Ministry of Economic Affairs, and the Foundation for Technical Research (STW).

[1] E. Desurvire, Sci. Am. January, 114 (1992).
[2] A. M. Glass, Phys. Today October, 34 (1993).
[3] E. Desurvire, Phys. Today January , 27 (1994).
[4] S. Hüfner, *Optical Spectra of Transparent Rare-Earth Compounds* (Academic, New York, 1980).
[5] Y. Yan, A. J. Faber, and H. de Waal, J. Non-Cryst. Solids **181**, 283 (1995).
[6] E. Snoeks, P. G. Kik, and A. Polman, Opt. Mater. (to be published).
[7] F. Auzel, J. Lumin. **45**, 341 (1990).
[8] P. Blixt, J. Nilsson, T. Carlnäs, and B. Jaskorzynska, IEEE Photon. Technol. Lett. **PTL-3**, 996 (1991).
[9] C. C. Ye, P. R. Morkel, E. R. Taylor, and D. N. Payne, in Proceedings of the 19th European Conference on Optical Communication, Montreux, September 12–16, 1993, Vol. 2, p. 73.
[10] C. B. Layne, W. H. Lowdermilk, and M. J. Weber, Phys. Rev. B **16**, 10 (1977).
[11] J. M. F. van Dijk and M. F. H. Schuurmans, J. Chem. Phys. **78**, 5317 (1983).
[12] E. Delevaque, T. Georges, M. Monerie, P. Lamouler, and J.-F. Bayon, IEEE Photon. Technol. Lett. **PTL-5**, 73 (1993).
[13] R. S. Quimby, W. J. Miniscalco, and B. Thompson, Proc. SPIE **2073**, 2 (1993).
[14] J. Nilsson, P. Blixt, B. Jaskorzynska, and J. Babonas, J. Lightwave Technol. **13**, 341 (1993).
[15] C. G. Atkins, J. R. Armitage, R. Wyatt, B. J. Ainslie, and S. P. Craig-Ryan, Opt. Commun. **73**, 217 (1989).
[16] R. S. Quimby, W. J. Miniscalco, and B. Thompson, Proc. SPIE **1789**, 50 (1993).
[17] A. J. Silversmith, W. Lenth, and R. M. Mcfarlane, Appl. Phys. Lett. **51**, 1977 (1987).
[18] S. A. Pollack and D. B. Chang, J. Appl. Phys. **64**, 2885 (1988).
[19] D. C. Yeh, W. A. Sibley, I. Schneider, R. S. Afzal, and I. Aggarwal, J. Appl. Phys. **69**, 1648 (1991).
[20] P. Xie and S. C. Rand, Opt. Lett. **17**, 1198 (1992).
[21] M. P. Hehlen, G. Frei, and H. U. Güdel, Phys. Rev. B **50**, 16 264 (1994).
[22] A. C. Tropper, J. N. Carter, R. D. T. Lauder, D. C. Hanna, S. T. Davey, and D. Szebesta, J. Opt. Soc. Am. B **11**, 886 (1994).
[23] M. Lui, R. A. MacFarlane, D. Yap, and D. Lederman, Electron. Lett. **29**, 172 (1993).
[24] L. Zhang, P. D. Townsend, P. J. Chandler, and A. J. Silversmith, Electron. Lett. **30**, 1063 (1994).
[25] P. Villars and L. D. Calvert, *Pearson's Handbook of Crystallographic Data for Intermetallic Phases* (American Society for Metals, Metals Park, OH, 1986), pp. 1047 and 2177, and references therein.
[26] A. Polman, D. C. Jacobson, D. J. Eaglesham, R. C. Kistler, and J. M. Poate, J. Appl. Phys. **70**, 3778 (1991).
[27] G. N. van den Hoven, E. Snoeks, A. Polman, J. W. M. van Uffelen, Y. S. Oei, and M. K. Smit, Appl. Phys. Lett. **62**, 3065 (1993).
[28] M. K. Smit, G. A. Acket, and C. J. van der Laan, Thin Solid Films Electron. Opt. **138**, 171 (1986).
[29] M. K. Smit, Ph.D. thesis, Delft University of Technology, 1991.
[30] C. van Dam, J. W. M. van Uffelen, M. K. Smit, G. N. van den Hoven, and A. Polman, in Proceedings of the 7th European Conference on Integrated Optics, Delft, April 3–6, 1995, p. 125.
[31] G. N. van den Hoven, A. Polman, C. van Dam, J. W. M. van Uffelen, and M. K. Smit (unpublished).
[32] G. N. van den Hoven, J. A. van der Elsken, A. Polman, C. van Dam, J. W. M. van Uffelen, and M. K. Smit (unpublished).
[33] W. Q. Shi, M. Bass, and M. Birnbaum, J. Opt. Soc. Am. B **7**, 1456 (1990).
[34] G. Nykolak, P. C. Becker, J. Shmulovich, Y. H. Wong, D. J. DiGiovanni, and A. J. Bruce, IEEE Photon. Technol. Lett. **PTL-5**, 1014 (1993).
[35] E. Snoeks, G. N. van den Hoven, A. Polman, B. Hendriksen, M. B. J. Diemeer, and F. Priolo, J. Opt. Soc. Am. B **12**, 1468 (1995).
[36] H. Schober, D. Strauch, and B. Dorner, Z. Phys. B **92**, 273 (1993).
[37] P. Blixt, J. Nilsson, J. Babonas, and B. Jaskorzynska (unpublished).
[38] J. E. Román, M. Hempstead, C. C. Ye, P. Camy, P. Laborde, and C. Lerminiaux, Appl. Phys. Lett. **67**, 470 (1995).
[39] A. M. Vredenberg and J. Shmulovich (unpublished).
[40] G. Nykolak, M. Haner, P. C. Becker, J. Shmulovich, and Y. H. Wong, IEEE Photon. Technol. Lett. **PTL-5**, 1185 (1993).
[41] K. Hattori, T. Kitagawa, M. Oguma, Y. Ohmori, and M. Horiguchi, Electron. Lett. **30**, 856 (1994).
[42] R. Brinkmann, I. Baumann, M. Dinand, W. Sohler, and H. Suche, IEEE J. Quantum Electron. **QE-30**, 2356 (1994).

[43] M. Hempstead, J. E. Román, C. C. Ye, J. S. Wilkinson, P. Camy, P. Laborde, and C. Lerminiaux, in Proceedings of the 7th European Conference on Integrated Optics, Delft, April 3–6, 1995, p. 233.
[44] D. Barbier, P. Gastaldo, B. Hyde, J. M. Jouanno, and A. Kevorkian, in Proceedings of the 7th European Conference on Integrated Optics, Delft, April 3–6, 1995, p. 241.
[45] F. Di Pasquale and M. Federighi, IEEE J. Quantum Electron. **QE-30**, 2127 (1994).
[46] G. N. van den Hoven, E. Snoeks, A. Polman, C. van Dam, J. W. M. van Uffelen, and M. K. Smit, in Proceedings of the 7th European Conference on Integrated Optics, Delft, April 3–6, 1995, p. 229.
[47] G. N. van den Hoven, R. J. I. M. Koper, A. Polman, C. van Dam, J. W. M. van Uffelen, and M. K. Smit (unpublished).